Dynamics of the binary asteroid (379) Huenna

Frédéric Vachier, Benoit Carry, Jérôme Berthier

Dynamics of the binary asteroid (379) Huenna

*Corresponding author
frederic.vachier@obspm.fr (F. Vachier)
ORCID(s): 0000-0002-4289-4466 (F. Vachier); 0000-0001-5242-3089 (B. Carry); 0000-0003-1846-6485 (J. Berthier)

Frédéric Vachier[a,*], Benoit Carry[b] and Jérôme Berthier[a]

[a] IMCCE, Observatoire de Paris, PSL Research University, CNRS, Sorbonne Universités, UPMC Univ Paris 06, Univ. Lille, France
[b] Université Côte d'Azur, Observatoire de la Côte d'Azur, CNRS, Laboratoire Lagrange, France

ARTICLE INFO

Keywords:
dynamics
external perturbers
bulk density

ABSTRACT

We aim at studying the dynamical system of the asteroid (379) Huenna and its satellite, for which a discrepancy between its predicted and observed position was reported by DeMeo et al. (2011, Icarus, 212). We compile all the available images of the system acquired with large ground-based telescopes equipped with adaptive-optics fed camera. Based on these 40 observations covering 11 years, we determine the orbit of the satellite which is strongly affected by the gravitationnal influence of the Sun, as opposed to most satellites of large main-belt asteroids. Combining the mass of Huenna with a compilation of diameter estimates from the literature, we revise the estimate of its bulk density to $\mathbf{1491 \pm 249}\,\mathrm{kg \cdot m^{-3}}$, consistent with its spectral classification as a P-type asteroid.

1. Introduction

Owing to their small size, asteroids had little, if any, geophysical evolution over the history of the Solar system after their initial accretion phase some 4.6 Gyr ago. Their orbital environment, dominated by collisions, however led to an important evolution of their physical properties such as spin, shape, and internal structure via shock-induced fractures. Asteroids are nevertheless the most pristine remnants of the early stages of the inner Solar system, and as such, they are used to constrain the models of formation and evolution of planetesimals from which terrestrial planets formed (Morbidelli et al., 2015; Clement et al., 2020)

Understanding their compositions, and how these distribute is key in that respect (DeMeo and Carry, 2014). The composition of asteroids is generally derived from photometry and spectroscopy compared with laboratory samples (Reddy et al., 2015). These are, however, sensitive to a thin surface layer only, which composition may or may be not related to the bulk composition of the asteroid. An obvious example is the differentiated asteroid (4) Vesta (McCord et al., 1970), but partially differentiated bodies could be common (Elkins-Tanton et al., 2011; Bryson et al., 2019). Asteroid bulk density is the sole remote-sensing quantity that can tells us about asteroid interiors, and provide hints on bulk composition (Scheeres et al., 2015).

The first and most difficult quantity to measure to derive an asteroid density is its mass. The only exception is the modeling of lightcurves of mutual events (eclipses and occultations) which provides the density without measuring the asteroid mass (nor volume, see Pravec et al., 2006; Scheirich and Pravec, 2009; Carry et al., 2015). In all cases, the most precise mass estimates (few percent accuracy) have been derived studying binary asteroids, or during spacecraft encounters (Pätzold et al., 2011; Pajuelo et al., 2018). Other determinations, relying on the modeling of the long-distance gravitational influence of the target asteroids on other small asteroids, have provided many more determination but with low precision to date (Zielenbach, 2011). There are currently about 300 small bodies with a mass determination (Carry, 2012).

We focus here on the asteroid (379) Huenna, around which a satellite was discovered in 2003 by Margot (2003). A dynamical solution for the orbit of the satellite was published by Marchis et al. (2008), providing the mass of Huenna. However, the observation in 2009 of Huenna's satellite for spectroscopic purposes revealed a clear offset (0.5″, about 680 km) between the predicted and observed positions (DeMeo et al., 2011), requiring an updated dynamical solution. A dynamical solution has indeed been recently published by Emelyanov and Drozdov (2020) based on the aforemetionned observations. Aware of additional observations present in archives, we collected images of Huenna's system as acquired by large ground-based telescopes in Section 2. We then describe the dynamical solution in Section 3, and discuss its implications in Section 4.

2. Observations and data reduction

We collect all the high angular-resolution images of Huenna taken with ground-based telescopes equipped with adaptive-optics (AO) cameras: ESO VLT and W. M. Keck. The data span **27** different epochs, with multiple images each, over **11** years from **August 2003** to **December 2014**. This data set includes the discovery observations of Margot (2003), those used by Marchis et al. (2008), the discrepant observation reported by DeMeo et al. (2011), and public data from the archives of the Keck (Keck engineering time and programs C257N2L, C192N2, PI M. Brown) and VLT telescopes (program 089.C-0944, PI F. Marchis).

The images from the VLT were acquired with NACO (NAOS-CONICA, Lenzen et al., 2003; Rousset et al., 2003), and those at Keck with NIRC2 (Near-InfraRed

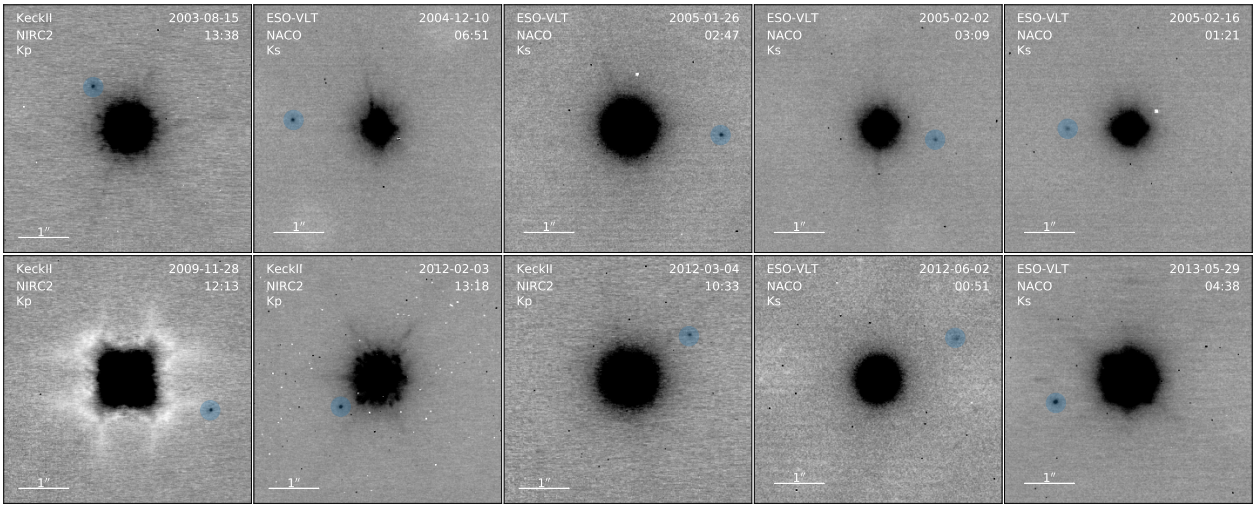

Figure 1: Examples of AO images. The small blue circles indicate the position of the satellite. North is up and East is left.

Camera 2, van Dam et al., 2004; Wizinowich et al., 2000). We reduce the AO imaging data with a standard data processing protocol (sky subtraction, bad-pixel identification and correction, and flat-field correction), using in-house routines (see Carry et al., 2008). The reduced images were processed to subtract the bright halo surrounding Huenna to enhance the detectability of its satellite (see Pajuelo et al., 2018, for details). The measured positions of the satellite are listed in Table 1, and we present a few examples in Figure 1.

3. Orbit of the satellite

We use all **40** positions of the satellite with respect to Huenna on the plane of the sky to characterize its orbital properties. We use the `Genoid` algorithm to find the set of dynamical parameters (mass, semi-major axis, eccentricity, inclination, longitude of the node, argument of pericenter, and time of passage to pericenter) that best fit the observations (see Vachier et al., 2012; Berthier et al., 2014; Carry et al., 2019, 2021, for a detailed description of the algorithm and application to different systems).

`Genoid` explores the parameter space by successives generations of suites of test solutions (called individuals). Each test solution consists in the set of dynamical parameters, and is compared with observations through numerical integration of the system, with the following metric:

$$\chi^2 = \sum_{i=1}^{N} \left[\left(\frac{X_{o,i} - X_{c,i}}{\sigma_{x,i}} \right)^2 + \left(\frac{Y_{o,i} - Y_{c,i}}{\sigma_{y,i}} \right)^2 \right] \quad (1)$$

where N is the number of observations, and X_i and Y_i are the relative positions between the satellite and Huenna along the right ascension and declination, respectively. The indices o and c stand for observed and computed positions, and σ are the measurement uncertainties.

At each generation, the individuals with the lowest χ^2 are used to generate the individuals of the following generation, by randomly mixing their parameters (like sexual reproduction mixes genes). At each generation, the best solution is also used as initial condition to search for the local minimum by gradient descent. The algorithm stops after a given number of generations, or when the χ^2 achieved by several generations does not evolve anymore.

The combination of both a large grid search and a gradient descent ensures finding the best global dynamical solution. The numerical integration is handled by `eproc`, the library of ephemerides computation behind all the Virtual Observatory Web services of the IMCCE (e.g., `SkyBoT`, `Miriade`, Berthier et al., 2006, 2008, 2016). As such, it is a one body integrator perturbed by N-bodies and has been extensively tested.

The numerical model used here consists in Huenna and its satellite, and the Sun. The case of Huenna differs from other large asteroids with satellite for which the perturbation by the Sun (or any planet) is negligible. Recent studies revealed purely Keplerian motions around (22) Kalliope, (31) Euphrosyne, (41) Daphne, (87) Sylvia, (107) Camilla, (130) Elektra, and (317) Roxane (Drummond et al., 2021; Yang et al., 2020; Carry et al., 2019, 2021; Berthier et al., 2014; Beauvalet and Marchis, 2014; Pajuelo et al., 2018; Yang et al., 2016). Considering the distribution of the separation between asteroids and their satellites (Fig. 2, data from Johnston 2019), only the outer satellite of (3749) Balam and the satellite of (379) Huenna are distant. The satellites of other bodies are located much deeper into their respective Hill spheres.

The influence of the Sun on the position of the satellite of Huenna is well above the typical precision of

Table 1
Astrometry of the satellite of Huenna. Date, mid-observing time (UTC), telescope, camera, filter, astrometry (X is aligned with Right Ascension, and Y with Declination, and o and c indices stand for observed and computed positions), uncertainty (σ), and photometry (magnitude difference ΔM with uncertainty δM) are reported.

Date	UTC	Tel.	Cam.	Filter	X_o (mas)	Y_o (mas)	X_{o-c} (mas)	Y_{o-c} (mas)	σ (mas)	ΔM (mag)	δM (mag)
2003-08-14	13:04:25.9	Keck-II	NIRC2	H	501	737	1	3	10.00	8.14	0.56
2003-08-14	14:07:52.8	Keck-II	NIRC2	H	506	737	-2	0	10.00	7.76	0.27
2003-08-15	13:34:46.6	Keck-II	NIRC2	Kp	693	838	1	0	10.00	6.98	0.07
2003-08-15	13:38:59.6	Keck-II	NIRC2	Kp	696	841	3	3	10.00	7.13	0.06
2003-08-17	14:53:55.0	Keck-II	NIRC2	Kp	1070	1028	1	-7	10.00	7.10	0.11
2003-08-18	14:19:56.0	Keck-II	NIRC2	Kp	1243	1116	2	-6	10.00	6.94	0.03
2004-12-08	07:08:31.3	ESO VLT	NACO	Ks	1783	130	4	4	13.30	7.43	0.80
2004-12-09	06:29:18.8	ESO VLT	NACO	Ks	1759	147	14	-2	13.30	6.55	0.41
2004-12-09	06:41:52.7	ESO VLT	NACO	Ks	1743	146	-1	-3	13.30	6.88	0.03
2004-12-10	06:45:20.8	ESO VLT	NACO	Ks	1702	176	1	1	13.30	6.37	0.56
2004-12-10	06:51:28.8	ESO VLT	NACO	Ks	1697	174	-2	0	13.30	6.67	0.03
2004-12-14	05:28:42.9	ESO VLT	NACO	Ks	1447	264	-1	2	13.30	6.65	0.07
2004-12-14	07:08:56.9	ESO VLT	NACO	Ks	1448	266	5	2	13.30	6.73	0.05
2004-12-15	05:20:24.8	ESO VLT	NACO	Ks	1370	285	1	3	13.30	6.87	0.13
2004-12-28	05:36:53.1	ESO VLT	NACO	Ks	-21	396	3	3	13.30	7.06	0.32
2004-12-28	07:41:12.8	ESO VLT	NACO	Ks	-41	397	-6	4	13.30	6.96	0.43
2004-12-29	05:13:34.3	ESO VLT	NACO	Ks	-141	391	0	0	13.30	6.28	0.00
2005-01-18	03:58:33.8	ESO VLT	NACO	Ks	-1924	65	4	7	13.30	7.03	0.07
2005-01-18	06:17:33.1	ESO VLT	NACO	Ks	-1931	56	0	1	13.30	6.72	0.13
2005-01-21	02:25:25.0	ESO VLT	NACO	Ks	-1991	-15	-4	0	13.30	6.79	0.51
2005-01-25	04:51:31.4	ESO VLT	NACO	Ks	-1916	-110	-2	0	13.30	7.44	0.00
2005-01-26	02:47:39.2	ESO VLT	NACO	Ks	-1868	-127	0	2	13.30	6.88	0.03
2005-01-26	05:10:41.1	ESO VLT	NACO	Ks	-1860	-127	3	3	13.30	7.42	0.28
2005-01-27	03:10:50.5	ESO VLT	NACO	Ks	-1799	-146	7	2	13.30	7.13	0.20
2005-01-28	03:04:35.7	ESO VLT	NACO	Ks	-1734	-166	-1	1	13.30	6.74	0.34
2005-01-28	03:13:54.0	ESO VLT	NACO	H	-1735	-159	-3	7	13.30	7.37	0.15
2005-02-02	03:09:16.2	ESO VLT	NACO	Ks	-1147	-222	1	0	13.30	7.09	0.03
2005-02-02	05:09:29.4	ESO VLT	NACO	Ks	-1134	-225	2	-3	13.30	7.00	0.08
2005-02-04	02:41:04.7	ESO VLT	NACO	Ks	-823	-223	5	0	13.30	7.02	0.20
2005-02-04	04:05:56.8	ESO VLT	NACO	Ks	-819	-224	0	0	13.30	6.84	0.12
2005-02-16	01:21:08.5	ESO VLT	NACO	Ks	1221	-4	-3	-2	13.30	6.72	0.27
2009-11-28	12:13:35.1	Keck-II	NIRC2	Kp	-1672	-616	-4	4	10.00	7.16	0.08
2009-11-28	12:51:36.2	Keck-II	NIRC2	Kp	-1673	-615	-7	3	10.00	6.97	0.03
2012-02-03	13:18:43.9	Keck-II	NIRC2	Kp	740	-551	-7	-3	10.00	6.94	0.43
2012-02-03	13:33:28.7	Keck-II	NIRC2	Kp	739	-552	-8	-5	10.00	6.98	0.09
2012-03-04	10:33:13.8	Keck-II	NIRC2	Kp	-1225	894	4	19	10.00	7.37	0.28
2012-03-29	07:16:52.3	Keck-II	NIRC2	Kp	-1881	656	0	5	10.00	6.93	0.03
2012-06-02	00:51:58.5	ESO VLT	NACO	Ks	-1568	825	-12	-16	13.30	7.01	0.31
2014-11-10	07:16:10.7	Keck-II	NIRC2	Ks	3079	1085	-5	-16	10.00	1.65	0.06
2014-12-07	05:38:57.2	Keck-II	NIRC2	Ks	-554	-585	-2	-2	10.00	6.65	0.01
						Average	0	0		6.86	0.18
						Standard deviation	4	6		0.90	0.17

measurements, around 0.01″ (Table 1). By comparing the best-fit solution (see below) including the Sun and a simple Keplerian orbit, we find a root mean-square residual of 0.477″ over the period of 11 years covered by the observations, the two orbit diverging with time (Figure 3). The second-largest external perturber is Jupiter, but only contributes at the level of 0.0001″ and we neglect it in our dynamical model.

We present in Table 2 the best-fitting orbital solution, providing a root mean-square deviation of only **5.4** milli-arseconds (mas). This orbit significantly differs from the original dynamical solution of Marchis et al. (2008). While the orientation of the orbit (node, inclination, pericenter) is similar within a few degrees, the orbital period strongly disagree: $\mathbf{80.2 \pm 0.01}$ d here, compared to the previous value of $\mathbf{87.6 \pm 0.26}$ d ; i.e., an increase of **9%**, at more than $\mathbf{28\,\sigma}$.

Four arguments argue in favor of the revised solu-

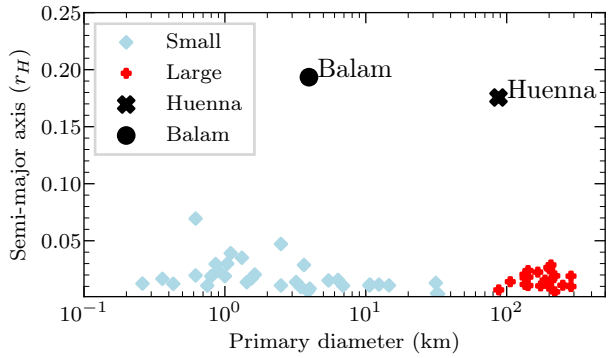

Figure 2: Semi-major axes of binary asteroids (expressed in radius of the Hill's sphere: r_H) as function of the diameter of the main component. The population is split into small (blue) and large (red) systems, using a diameter of 30 km to separate them.

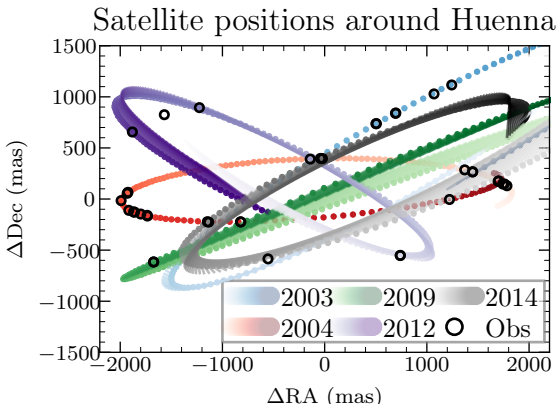

Figure 3: Comparison of the predicted position from a Keplerian orbit (fit over all 31 positions between 2003 and 2005 with a RMS of 3.6 mas only) and the orbit including the influence of the Sun. The black dots are the observations. The predictions of the two orbits are connected by lines, color-coded by epoch. The later the epoch the larger the difference.

tion: the agreement within 3 σ between our dynamical solution and the recent study by Emelyanov and Drozdov (2020), the small residuals obtained here, the poor prediction of previous solution for the 2009 observation reported by DeMeo et al. (2011), and the time coverage of only **70** d used by Marchis et al. (2008), i.e., shorter than an orbital period.

4. Discussion

The revised dynamical solution implies a significantly larger mass (36%) compared to the previous determination (Marchis et al., 2008). In what follow, we assume that all the mass of the system is in Huenna, owing to the small size of its satellite (see below). We compile all the diameter estimates available in the literature in Table 3, and estimate an average diameter of **87.5**± **8.2** km. There is a significant spread among estimates, resulting in 10% uncertainty. This is expected for estimates based on the analysis of mid-infrared fluxes using a spherical assumption on the shape of asteroids (Mainzer et al., 2011; Carry, 2012; Usui et al., 2014; Herald et al., 2020). The updated mass and diameter estimates imply a bulk density of **1491**± **249** kg·m^{-3}. This density is typical for a P-type (see, e.g., Carry, 2012; Berthier et al., 2014; Pajuelo et al., 2018; Carry et al., 2021; Vernazza et al., 2021). The diameter estimates are, however, only based on disk-integrated measurements, and the density estimate should hence be interpreted with caution.

Assuming that Huenna and its satellite have the same albedo (a reasonable assumption considering their similar spectra, see DeMeo et al., 2011), their apparent magnitude difference of **6.9**± **0.9** (Table 1) implies a diameter of 3.72± 0.60 km only for the satellite. It is thus one of the smallest satellites of large (50+ km) asteroids known to date, with Daphne, Elektra, and Minerva (Marchis et al., 2013; Yang et al., 2016; Carry et al., 2019).

Small satellites of large asteroids are thought to form in giant collisions (Durda et al., 2004; Margot et al., 2015), and share common properties. Their orbits tend to be equatorial, circular, in the direct sense, and deep within their Hill spheres (**0.017** ± **0.002**). The peculiar properties of the satellite of Huenna, especially its eccentricity and large semi-major axis, questions its origin, or evolution. While the likelihood of an origin by capture is low (Weidenschilling et al., 1989), what excited its orbit and increased its eccentricity and semi-major axis if formed like other satellites of large asteroids? The spin axis of Huenna is not known, and lightcurve observations of Huenna to determine it will help understanding the geometry of the system: whether the mutual orbit is equatorial or tilted.

5. Conclusion

We searched for adaptive-optics images of the asteroid (379) Huenna in the archives of large ground-based telescopes. We measured **40** positions of the satellite with respect to Huenna taken over 11 years. From these positions, we determined the dynamics of the satellite, solving the miss-match between previously published orbit and an observation in 2009. We derived a new estimate of the mass of Huenna. Combined with its average diameter computed from estimates reported in the literature, we determined a density of **1491** ± **249** kg·m^{-3}, typical of the P-types asteroids like Huenna. The satellite is on an eccentricity orbit, far from Huenna, which contrasts with the properties of most known satellites around large main-belt asteroids. A physical characterization of Huenna, and in particular of its spin axis, is required to study further the origin of this system.

Table 2
Orbital elements and state vector (centered on Huenna) of the satellite of Huenna, expressed in EQJ2000: orbital period P, semi-major axis a, eccentricity e, inclination i, longitude of the ascending node Ω, argument of pericenter ω, time of pericenter t_p. The number of observations and RMS between predicted and observed positions are also provided. Finally, we report the system total mass M, the ecliptic J2000 coordinates of the orbital pole (λ_p, β_p), and the equatorial J2000 coordinates of the orbital pole (α_p, δ_p). Uncertainties are given at 3-σ.

Observing data set		
Number of observations	40	
Time span (days)	4133	
RMS (mas)	5.4	
Orbital elements EQJ2000		
P (day)	80.216	$\pm$ 0.015
a (km)	3487.9	$\pm$ 41.4
e	0.283	$\pm$ 0.010
i (^{o})	151.19	$\pm$ 0.68
Ω (^{o})	204.53	$\pm$ 1.19
ω (^{o})	278.9	$\pm$ 1.5
t_p (JD)	2452930.961	$\pm$ 0.31
State vector EQJ2000		
x (m)	-3 228 767.0	
y (m)	-621 087.4	
z (m)	426 401.0	
v_x (m/s)	-1.2471	
v_y (m/s)	2.6316	
v_z (m/s)	1.6019	
Derived parameters		
M ($\times 10^{17}$ kg)	5.23	$\pm$ 0.19
α_p, δ_p (^{o})	114.5, -61.2	$\pm$ 1.2, 0.7
λ_p, β_p (^{o})	161.8, -77.8	$\pm$ 3.4, 0.5

Table 3
Diameter estimates of Huenna compiled from the literature.

Diameter (km)	Method	Reference
92.33 $\pm$ 1.70	STM	Tedesco et al. (2001)
103.01 $\pm$ 4.31	NEATM	Ryan and Woodward (2010)
82.02 $\pm$ 2.56	STM	Ryan and Woodward (2010)
87.47 $\pm$ 2.36	NEATM	Masiero et al. (2011)
104.56 $\pm$ 1.88	NEATM	Masiero et al. (2012)
87.34 $\pm$ 9.06	NEATM	Pravec et al. (2012)
82.35 $\pm$ 1.08	NEATM	Hasegawa et al. (2013)
88.00 $\pm$ 9.00	NEATM	Alí-Lagoa et al. (2013)
84.79 $\pm$ 1.56	NEATM	Masiero et al. (2014)
85.70 $\pm$ 8.57	NEATM	Alí-Lagoa et al. (2016)
85.82 $\pm$ 23.24	NEATM	Nugent et al. (2015)
71.59 $\pm$ 18.01	NEATM	Nugent et al. (2016)
86.18 $\pm$ 25.86	NEATM	Nugent et al. (2016)
75.77 $\pm$ 15.15	NEATM	Alí-Lagoa et al. (2018)
87.25 $\pm$ 17.45	NEATM	Alí-Lagoa et al. (2018)
95.95 $\pm$ 9.59	NEATM	Alí-Lagoa et al. (2018)

Acknowledgments

Some of the work presented here is based on observations collected at the European Organisation for Astronomical Research in the Southern Hemisphere under ESO program 074.C-0052 and 089.C-0944 (PI Marchis).

Some of the data presented herein were obtained at the W.M. Keck Observatory, which is operated as a scientific partnership among the California Institute of Technology, the University of California and the National Aeronautics and Space Administration. The Observatory was made possible by the generous financial support of the W.M. Keck Foundation. This research has made use of the Keck Observatory Archive (KOA), which is operated by the W. M. Keck Observatory and the NASA Exoplanet Science Institute (NExScI), under contract with the National Aeronautics and Space Administration. The authors wish to recognize and acknowledge the very significant cultural role and reverence that the summit of Mauna Kea has always had within the indigenous Hawaiian community.

B. Carry was supported by CNRS/INSU/PNP. The authors acknowledge the use of the Virtual Observatory tools Miriade [1] (Berthier et al., 2008), TOPCAT [2], and STILTS [3] (Taylor, 2005). This research used the SSOIS [4] facility of the Canadian Astronomy Data Centre operated by the National Research Council of Canada with the support of the Canadian Space Agency (Gwyn et al., 2012).

References

Alí-Lagoa, V., de León, J., Licandro, J., Delbó, M., Campins, H., Pinilla-Alonso, N., Kelley, M.S., 2013. Physical properties of B-type asteroids from WISE data. A&A 554, A71. doi:10.1051/0004-6361/201220680, arXiv:1303.5487.

Alí-Lagoa, V., Licandro, J., Gil-Hutton, R., Cañada-Assandri, M., Delbo', M., de León, J., Campins, H., Pinilla-Alonso, N., Kelley, M.S.P., Hanuš, J., 2016. Differences between the Pallas collisional family and similarly sized B-type asteroids. A&A 591, A14. doi:10.1051/0004-6361/201527660.

Alí-Lagoa, V., Müller, T.G., Usui, F., Hasegawa, S., 2018. The AKARI IRC asteroid flux catalogue: updated diameters and albedos. A&A 612, A85. doi:10.1051/0004-6361/201731806, arXiv:1712.07496.

Beauvalet, L., Marchis, F., 2014. Multiple asteroid systems (45) Eugenia and (87) Sylvia: Sensitivity to external and internal perturbations. Icarus 241, 13–25. doi:10.1016/j.icarus.2014.06.004.

Berthier, J., Carry, B., Vachier, F., Eggl, S., Santerne, A., 2016. Prediction of transits of Solar system objects in Kepler/K2 images: an extension of the Virtual Observatory service SkyBoT. MNRAS 458, 3394–3398. doi:10.1093/mnras/stw492.

Berthier, J., Hestroffer, D., Carry, B., Ďurech, J., Tanga, P., Delbo, M., Vachier, F., 2008. A Service of Position and Physical Ephemerides Computation Dedicated to the Small Bodies of the Solar System. LPI Contributions 1405, 8374.

[1] Miriade: http://vo.imcce.fr/webservices/miriade/
[2] TOPCAT: http://www.star.bris.ac.uk/ mbt/topcat/
[3] STILTS: http://www.star.bris.ac.uk/ mbt/stilts/
[4] SSOIS: http://www.cadc-ccda.hia-iha.nrc-cnrc.gc.ca/en/ssois

Berthier, J., Vachier, F., Marchis, F., Ďurech, J., Carry, B., 2014. Physical and dynamical properties of the main belt triple Asteroid (87) Sylvia. Icarus 239, 118–130. doi:10.1016/j.icarus.2014.05.046.

Berthier, J., Vachier, F., Thuillot, W., Fernique, P., Ochsenbein, F., Genova, F., Lainey, V., Arlot, J.E., 2006. SkyBoT, a new VO service to identify Solar System objects, in: Gabriel, C., Arviset, C., Ponz, D., Enrique, S. (Eds.), Astronomical Data Analysis Software and Systems XV, p. 367.

Bryson, J.F.J., Weiss, B.P., Getzin, B., Abrahams, J.N.H., Nimmo, F., Scholl, A., 2019. Paleomagnetic Evidence for a Partially Differentiated Ordinary Chondrite Parent Asteroid. Journal of Geophysical Research (Planets) 124, 1880–1898. doi:10.1029/2019JE005951.

Carry, B., 2012. Density of asteroids. Planet. Space Sci. 73, 98–118. doi:10.1016/j.pss.2012.03.009.

Carry, B., Dumas, C., Fulchignoni, M., Merline, W.J., Berthier, J., Hestroffer, D., Fusco, T., Tamblyn, P., 2008. Near-Infrared Mapping and Physical Properties of the Dwarf-Planet Ceres. A&A 478, 235–244. doi:10.1051/0004-6361:20078166.

Carry, B., Matter, A., Scheirich, P., Pravec, P., Molnar, L., Mottola, S., Carbognani, A., Jehin, E., Marciniak, A., Binzel, R.P., DeMeo, F., Birlan, M., Delbo, M., Barbotin, E., Behrend, R., Bonnardeau, M., Colas, F., Farissier, P., Fauvaud, M., Fauvaud, S., Gillier, C., Gillon, M., Hellmich, S., Hirsch, R., Leroy, A., Manfroid, J., Montier, J., Morelle, E., Richard, F., Sobkowiak, K., Strajnic, J., Vachier, F., 2015. The small binary asteroid (939) Isberga. Icarus 248, 516–525. doi:10.1016/j.icarus.2014.11.002.

Carry, B., Vachier, F., Berthier, J., Marsset, M., Vernazza, P., Grice, J., Merline, W.J., Lagadec, E., Fienga, A., Conrad, A., Podlewska-Gaca, E., Santana-Ros, T., Viikinkoski, M., Hanuš, J., Dumas, C., Drummond, J.D., Tamblyn, P.M., Chapman, C.R., Behrend, R., Bernasconi, L., Bartczak, P., Benkhaldoun, Z., Birlan, M., Castillo-Rogez, J., Cipriani, F., Colas, F., Drouard, A., Ďurech, J., Enke, B.L., Fauvaud, S., Ferrais, M., Fetick, R., Fusco, T., Gillon, M., Jehin, E., Jorda, L., Kaasalainen, M., Keppler, M., Kryszczynska, A., Lamy, P., Marchis, F., Marciniak, A., Michalowski, T., Michel, P., Pajuelo, M., Tanga, P., Vigan, A., Warner, B., Witasse, O., Yang, B., Zurlo, A., 2019. Homogeneous internal structure of CM-like asteroid (41) Daphne. A&A 623, A132. doi:10.1051/0004-6361/201833898, arXiv:1901.01890.

Carry, B., Vernazza, P., Vachier, F., Neveu, M., Berthier, J., Hanuš, J., Ferrais, M., Jorda, L., Marsset, M., Viikinkoski, M., Bartczak, P., Behrend, R., Benkhaldoun, Z., Birlan, M., Castillo-Rogez, J., Cipriani, F., Colas, F., Drouard, A., Dudziński, G.P., Desmars, J., Dumas, C., Ďurech, J., Fetick, R., Fusco, T., Grice, J., Jehin, E., Kaasalainen, M., Kryszczynska, A., Lamy, P., Marchis, F., Marciniak, A., Michalowski, T., Michel, P., Pajuelo, M., Podlewska-Gaca, E., Rambaux, N., Santana-Ros, T., Storrs, A., Tanga, P., Vigan, A., Warner, B., Wieczorek, M., Witasse, O., Yang, B., 2021. Evidence for differentiation of the most primitive small bodies. A&A 650, A129. doi:10.1051/0004-6361/202140342, arXiv:2103.06349.

Clement, M.S., Morbidelli, A., Raymond, S.N., Kaib, N.A., 2020. A record of the final phase of giant planet migration fossilized in the asteroid belt's orbital structure. MNRAS 492, L56–L60. doi:10.1093/mnrasl/slz184, arXiv:1912.02833.

van Dam, M.A., Le Mignant, D., Macintosh, B., 2004. Performance of the Keck Observatory adaptive-optics system. Applied Optics 43, 5458–5467.

DeMeo, F., Carry, B., Marchis, F., Birlan, M., Binzel, R.P., Bus, S.J., Descamps, P., Nedelcu, A., Busch, M., Bouy, H., 2011. A spectral comparison of (379) Huenna and its satellite. Icarus 212, 677–681. doi:10.1016/j.icarus.2011.02.002.

DeMeo, F.E., Carry, B., 2014. Solar System evolution from compositional mapping of the asteroid belt. Nature 505, 629–634. doi:10.1038/nature12908.

Drummond, J.D., Merline, W.J., Carry, B., Conrad, A., Tamblyn, P., Enke, B., Christou, J., Dumas, C., Chapman, C.R., Durda, D.D., Owen, W.M., Grundy, W.M., Reynolds, O.R., Buckman, M.D., 2021. The orbit of asteroid (317) Roxane's satellite Olympias from Gemini, Keck, VLT and the SOR, and (22) Kalliope's Linus from the SOR. Icarus 358, 114275. doi:10.1016/j.icarus.2020.114275.

Durda, D.D., Bottke, W.F., Enke, B.L., Merline, W.J., Asphaug, E., Richardson, D.C., Leinhardt, Z.M., 2004. The formation of asteroid satellites in large impacts: results from numerical simulations. Icarus 170, 243–257. doi:10.1016/j.icarus.2004.04.003.

Elkins-Tanton, L.T., Weiss, B.P., Zuber, M.T., 2011. Chondrites as samples of differentiated planetesimals. Earth and Planetary Science Letters 305, 1–10. doi:10.1016/j.epsl.2011.03.010.

Emelyanov, N.V., Drozdov, A.E., 2020. Determination of the orbits of 62 moons of asteroids based on astrometric observations. MNRAS 494, 2410–2416. doi:10.1093/mnras/staa784.

Gwyn, S.D.J., Hill, N., Kavelaars, J.J., 2012. Ssos: A moving-object image search tool for asteroid precovery. Publications of the Astronomical Society of the Pacific 124, 579. doi:10.1086/666462.

Hasegawa, S., Müller, T.G., Kuroda, D., Takita, S., Usui, F., 2013. The Asteroid Catalog Using AKARI IRC Slow-Scan Observations. PASJ 65, 34. doi:10.1093/pasj/65.2.34, arXiv:1210.7557.

Herald, D., Gault, D., Anderson, R., Dunham, D., Frappa, E., Hayamizu, T., Kerr, S., Miyashita, K., Moore, J., Pavlov, H., Preston, S., Talbot, J., Timerson, B., 2020. Precise astrometry and diameters of asteroids from occultations - a data set of observations and their interpretation. MNRAS 499, 4570–4590. doi:10.1093/mnras/staa3077, arXiv:2010.06086.

Johnston, W., 2019. Binary Minor Planets Compilation V3.0. NASA Planetary Data System. doi:10.26033/bb68-pw96.

Lenzen, R., Hartung, M., Brandner, W., Finger, G., Hubin, N.N., Lacombe, F., Lagrange, A.M., Lehnert, M.D., Moorwood, A.F.M., Mouillet, D., 2003. NAOS-CONICA first on sky results in a variety of observing modes. SPIE 4841, 944–952.

Mainzer, A., Grav, T., Masiero, J., Bauer, J., Wright, E., Cutri, R.M., McMillan, R.S., Cohen, M., Ressler, M., Eisenhardt, P., 2011. Thermal Model Calibration for Minor Planets Observed with Wide-field Infrared Survey Explorer/NEOWISE. ApJ 736, 100. doi:10.1088/0004-637X/736/2/100.

Marchis, F., Descamps, P., Berthier, J., Hestroffer, D., Vachier, F., Baek, M., Harris, A.W., Nesvorný, D., 2008. Main belt binary asteroidal systems with eccentric mutual orbits. Icarus 195, 295–316. doi:10.1016/j.icarus.2007.12.010.

Marchis, F., Vachier, F., Ďurech, J., Enriquez, J.E., Harris, A.W., Dalba, P.A., Berthier, J., Emery, J.P., Bouy, H., Melbourne, J., Stockton, A., Fassnacht, C.D., Dupuy, T.J., Strajnic, J., 2013. Characteristics and large bulk density of the C-type main-belt triple asteroid (93) Minerva. Icarus 224, 178–191. doi:10.1016/j.icarus.2013.02.018.

Margot, J.L., 2003. S/2003 (379) 1. IAU Circ. 8182, 1.

Margot, J.L., Pravec, P., Taylor, P., Carry, B., Jacobson, S., 2015. Asteroid Systems: Binaries, Triples, and Pairs. Univ. Arizona Press. pp. 355–374. doi:10.2458/azu_uapress_9780816532131-ch019.

Masiero, J.R., Grav, T., Mainzer, A.K., Nugent, C.R., Bauer, J.M., Stevenson, R., Sonnett, S., 2014. Main-belt Asteroids with WISE/NEOWISE: Near-infrared Albedos. ApJ 791, 121. doi:10.1088/0004-637X/791/2/121, arXiv:1406.6645.

Masiero, J.R., Mainzer, A.K., Grav, T., Bauer, J.M., Cutri, R.M., Dailey, J., Eisenhardt, P.R.M., McMillan, R.S., Spahr, T.B., Skrutskie, M.F., Tholen, D., Walker, R.G., Wright,

E.L., DeBaun, E., Elsbury, D., Gautier, IV, T., Gomillion, S., Wilkins, A., 2011. Main Belt Asteroids with WISE/NEOWISE. I. Preliminary Albedos and Diameters. ApJ 741, 68. doi:10.1088/0004-637X/741/2/68.

Masiero, J.R., Mainzer, A.K., Grav, T., Bauer, J.M., Cutri, R.M., Nugent, C., Cabrera, M.S., 2012. Preliminary Analysis of WISE/NEOWISE 3-Band Cryogenic and Post-cryogenic Observations of Main Belt Asteroids. ApJ 759, L8. doi:10.1088/2041-8205/759/1/L8, arXiv:1209.5794.

McCord, T.B., Adams, J.B., Johnson, T.V., 1970. Asteroid vesta: Spectral reflectivity and compositional implications. Science 168, 1445–1447. doi:10.1126/science.168.3938.1445.

Morbidelli, A., Walsh, K.J., O'Brien, D.P., Minton, D.A., Bottke, W.F., 2015. The Dynamical Evolution of the Asteroid Belt. pp. 493–507. doi:10.2458/azu_uapress_9780816532131-ch026.

Nugent, C.R., Mainzer, A., Bauer, J., Cutri, R.M., Kramer, E.A., Grav, T., Masiero, J., Sonnett, S., Wright, E.L., 2016. NEOWISE Reactivation Mission Year Two: Asteroid Diameters and Albedos. AJ 152, 63. doi:10.3847/0004-6256/152/3/63, arXiv:1606.08923.

Nugent, C.R., Mainzer, A., Masiero, J., Bauer, J., Cutri, R.M., Grav, T., Kramer, E., Sonnett, S., Stevenson, R., Wright, E.L., 2015. NEOWISE Reactivation Mission Year One: Preliminary Asteroid Diameters and Albedos. ApJ 814, 117. doi:10.1088/0004-637X/814/2/117, arXiv:1509.02522.

Pajuelo, M., Carry, B., Vachier, F., Marsset, M., Berthier, J., Descamps, P., Merline, W.J., Tamblyn, P.M., Grice, J., Conrad, A., Storrs, A., Timerson, B., Dunham, D., Preston, S., Vigan, A., Yang, B., Vernazza, P., Fauvaud, S., Bernasconi, L., Romeuf, D., Behrend, R., Dumas, C., Drummond, J.D., Margot, J.L., Kervella, P., Marchis, F., Girard, J.H., 2018. Physical, spectral, and dynamical properties of asteroid (107) Camilla and its satellites. Icarus 309, 134–161. doi:10.1016/j.icarus.2018.03.003, arXiv:1803.02722.

Pätzold, M., Andert, T.P., Asmar, S.W., Anderson, J.D., Barriot, J.P., Bird, M.K., Häusler, B., Hahn, M., Tellmann, S., Sierks, H., Lamy, P., Weiss, B.P., 2011. Asteroid 21 Lutetia: Low Mass, High Density. Science 334, 491. URL: http://www.sciencemag.org/content/334/6055/491.abstract, doi:10.1126/science.1209389.

Pravec, P., Harris, A.W., Kušnirák, P., Galád, A., Hornoch, K., 2012. Absolute magnitudes of asteroids and a revision of asteroid albedo estimates from WISE thermal observations. Icarus 221, 365–387. doi:10.1016/j.icarus.2012.07.026.

Pravec, P., Scheirich, P., Kušnirák, P., Šarounová, L., Mottola, S., Hahn, G., Brown, P.G., Esquerdo, G.A., Kaiser, N., Krzeminski, Z., Pray, D.P., Warner, B.D., Harris, A.W., Nolan, M.C., Howell, E.S., Benner, L.A.M., Margot, J.L., Galád, A., Holliday, W., Hicks, M.D., Krugly, Y.N., Tholen, D.J., Whiteley, R.J., Marchis, F., Degraff, D.R., Grauer, A., Larson, S., Velichko, F.P., Cooney, W.R., Stephens, R., Zhu, J., Kirsch, K., Dyvig, R., Snyder, L., Reddy, V., Moore, S., Gajdoš, Š., Világi, J., Masi, G., Higgins, D., Funkhouser, G., Knight, B., Slivan, S.M., Behrend, R., Grenon, M., Burki, G., Roy, R., Demeautis, C., Matter, D., Waelchli, N., Revaz, Y., Klotz, A., Rieugné, M., Thierry, P., Cotrez, V., Brunetto, L., Kober, G., 2006. Photometric survey of binary near-Earth asteroids. Icarus 181, 63–93. doi:10.1016/j.icarus.2005.10.014.

Reddy, V., Dunn, T., Thomas, C.A., Moskovitz, N., Burbine, T., 2015. Mineralogy and Surface Composition of Asteroids. Asteroids IV , na.

Rousset, G., Lacombe, F., Puget, P., Hubin, N.N., Gendron, E., Fusco, T., Arsenault, R., Charton, J., Feautrier, P., Gigan, P., Kern, P.Y., Lagrange, A.M., Madec, P.Y., Mouillet, D., Rabaud, D., Rabou, P., Stadler, E., Zins, G., 2003. NAOS, the first AO system of the VLT: on-sky performance. SPIE 4839, 140–149.

Ryan, E.L., Woodward, C.E., 2010. Rectified Asteroid Albedos and Diameters from IRAS and MSX Photometry Catalogs. AJ 140, 933–943. doi:10.1088/0004-6256/140/4/933.

Scheeres, D.J., Britt, D., Carry, B., Holsapple, K.A., 2015. Asteroid Interiors and Morphology. Univ. Arizona Press. pp. 745–766. doi:10.2458/azu_uapress_9780816532131-ch038.

Scheirich, P., Pravec, P., 2009. Modeling of lightcurves of binary asteroids. Icarus 200, 531–547. doi:10.1016/j.icarus.2008.12.001.

Taylor, M.B., 2005. TOPCAT & STIL: Starlink Table/VOTable Processing Software, in: Shopbell, P., Britton, M., Ebert, R. (Eds.), Astronomical Data Analysis Software and Systems XIV, p. 29.

Tedesco, E.F., Price, S.D., Egan, M.P., 2001. MIMPS, in: AAS/Division for Planetary Sciences Meeting Abstracts #33, p. 41.24.

Usui, F., Hasegawa, S., Ishiguro, M., Müller, T.G., Ootsubo, T., 2014. A comparative study of infrared asteroid surveys: IRAS, AKARI, and WISE. PASJ 66, 56. doi:10.1093/pasj/psu037, arXiv:1403.7854.

Vachier, F., Berthier, J., Marchis, F., 2012. Determination of binary asteroid orbits with a genetic-based algorithm. A&A 543, A68. doi:10.1051/0004-6361/201118408.

Vernazza, P., Ferrais, M., Jorda, L., Hanuš, J., Carry, B., Marsset, M., Brož, M., Fetick, R., Viikinkoski, M., Marchis, F., Vachier, F., Drouard, A., Fusco, T., Birlan, M., Podlewska-Gaca, E., Rambaux, N., Neveu, M., Bartczak, P., Dudziński, G., Jehin, E., Beck, P., Berthier, J., Castillo-Rogez, J., Cipriani, F., Colas, F., Dumas, C., Ďurech, J., Grice, J., Kaasalainen, M., Kryszczynska, A., Lamy, P., Le Coroller, H., Marciniak, A., Michalowski, T., Michel, P., Santana-Ros, T., Tanga, P., Vigan, A., Witasse, O., Yang, B., Antonini, P., Audejean, M., Aurard, P., Behrend, R., Benkhaldoun, Z., Bosch, J.M., Chapman, A., Dalmon, L., Fauvaud, S., Hamanowa, H., Hamanowa, H., His, J., Jones, A., Kim, D.H., Kim, M.J., Krajewski, J., Labrevoir, O., Leroy, A., Livet, F., Molina, D., Montaigut, R., Oey, J., Payre, N., Reddy, V., Sabin, P., Sanchez, A.G., Socha, L., 2021. VLT/SPHERE imaging survey of the largest main-belt asteroids: Final results and synthesis. A&A 654, A56. doi:10.1051/0004-6361/202141781.

Weidenschilling, S.J., Paolicchi, P., Zappala, V., 1989. Do asteroids have satellites? Asteroids II , 643–658.

Wizinowich, P.L., Acton, D.S., Lai, O., Gathright, J., Lupton, W., Stomski, Jr., P.J., 2000. Performance of the W.M. Keck Observatory Natural Guide Star Adaptive Optic Facility: the first year at the telescope, in: SPIE, pp. 2–13. doi:10.1117/12.390368.

Yang, B., Hanuš, J., Carry, B., Vernazza, P., Brož, M., Vachier, F., Rambaux, N., Marsset, M., Chrenko, O., Ševeček, P., Viikinkoski, M., Jehin, E., Ferrais, M., Podlewska-Gaca, E., Drouard, A., Marchis, F., Birlan, M., Benkhaldoun, Z., Berthier, J., Bartczak, P., Dumas, C., Dudziński, G., Ďurech, J., Castillo-Rogez, J., Cipriani, F., Colas, F., Fetick, R., Fusco, T., Grice, J., Jorda, L., Kaasalainen, M., Kryszczynska, A., Lamy, P., Marciniak, A., Michalowski, T., Michel, P., Pajuelo, M., Santana-Ros, T., Tanga, P., Vigan, A., Witasse, O., 2020. Binary asteroid (31) Euphrosyne: ice-rich and nearly spherical. A&A 641, A80. doi:10.1051/0004-6361/202038372, arXiv:2007.08059.

Yang, B., Wahhaj, Z., Beauvalet, L., Marchis, F., Dumas, C., Marsset, M., Nielsen, E.L., Vachier, F., 2016. Extreme AO Observations of Two Triple Asteroid Systems with SPHERE. ApJ 820, L35. doi:10.3847/2041-8205/820/2/L35, arXiv:1603.04435.

Zielenbach, W., 2011. Mass Determination Studies of 104 Large Asteroids. AJ 142, 120–128. doi:10.1088/0004-6256/142/4/120.

Graphical Abstract

Dynamics of the binary asteroid (379) Huenna

Frédéric Vachier,Benoit Carry,Jérôme Berthier

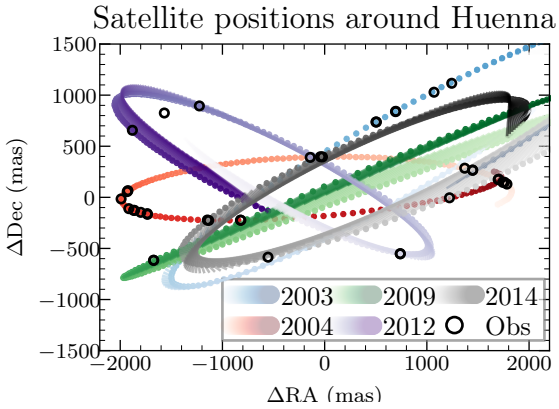

Highlights

Dynamics of the binary asteroid (379) Huenna

Frédéric Vachier,Benoit Carry,Jérôme Berthier

- We gather 40 observations of Huenna and its satellite
- We revise the published orbital elements of the satellite
- The satellite is distant from Huenna, differing from other satellites of large asteroids
- The density of Huenna is $\mathbf{1491} \pm \mathbf{249}\,\mathrm{kg \cdot m^{-3}}$